International Journal of Heat and Mass Transfer 55 (2012) 6881–6889

Contents lists available at SciVerse ScienceDirect

International Journal of Heat and Mass Transfer

journal homepage: www.elsevier.com/locate/ijhmt

Incipience of boiling on a wire

Jean-Charles Nardin [a], Cédric Poulain [b,*], Jérôme Duplat [c]

[a] Aix-Marseille Université - 13331 Marseille Cedex 03, France
[b] CEA, DEN, DM2S, STMF, F-38054 Grenoble, France
[c] SBT, UMR-E 9004 CEA / UJF-Grenoble 1, INAC, Grenoble F-38054, France

ARTICLE INFO

Article history:
Received 19 March 2012
Received in revised form 25 June 2012
Accepted 29 June 2012
Available online 31 July 2012

Keywords:
Nucleation
Boiling
Phase change
Acoustic
Bubble dynamics

ABSTRACT

The initial steps in the process of vaporisation of ethyl alcohol around a heated micrometric platinum wire are presented. A constant heat flux is imposed during a few milliseconds in the wire, elevating in turn the liquid temperature well above its saturation temperature until the first bubble is observed and expands before possibly collapsing. The bubble dynamics is tracked by high speed imaging as well as by acoustic emission during the bubble growth. We show that this nucleation process occurs for a fixed temperature $T^* = 465$ K (i.e. 114 K above saturation). The maximum volume and lifetime of this primary bubble are predicted by considering the energy budget between the amount of specific energy stored in the liquid and the latent heat consumed during the vaporisation process.

1. Introduction

When the thermodynamical conditions of a liquid bulk are modified such that the new equilibrium and stable state is the vapour phase, a local phase change is likely to be triggered. Whatever the thermodynamical pathway followed, this transition usually occurs locally in space and time via a nucleation process, in which one (possibly more) bubble grows with a rapid dynamic.

Basically, three different thermodynamic pathways can be explored to vary the chemical potential and enter the metastable region [1] at which nucleation must occur, leading to essentially three families of experiments:

Firstly, cavitation experiments, in which the pressure is lowered (at constant temperature) to put the liquid under tension, in most cases by acoustics or hydrodynamic means [1]. Recent work on cavitation has led to important breakthrough in the comprehension of homogeneous nucleation statistics. However strong discrepancies are still reported concerning the negative pressure threshold in pure liquids, namely water, between different methods (ultrasonic or hydrodynamic cavitation, artificial tree...) on the one hand, and the so called Classical Nucleation Theory (CNT) on the other [2–4].

Secondly, supersaturation experiments, consisting in increasing a dissolved gas concentration to modify the mixture's chemical potential and explore its metastability [5]. The unfortunately too rare experimental works reveal an important disagreement with theoretical predictions and for example, nucleation might be observed at concentration about 100 times smaller than expected by the CNT [6]. As shown by molecular dynamics simulations, neglecting the specific chemical interaction of the dissolved and solute molecules could be at the origin of this disagreement [7].

Finally, boiling experiments, in which the temperature of a pure liquid is increased above saturation (usually at constant pressure) is the third main way of experimenting nucleation, ubiquitous in everyday life.

Whatever the pathway, addressing the bubble dynamic at the onset of nucleation can teach us about the initial conditions with which this event proceeds, as well as a better comprehension of this very fast phenomenon. Here, we have chosen to address this problem in the framework of boiling. Indeed, the 'onset of boiling' represents the first multiphase event of the boiling process and the maximum temperature at which a liquid can be heated might be at play in other rapid phenomena such as the boiling crisis [8].

In this work, the onset of boiling is studied thanks to a long thin wire heated in a bulk of liquid. This configuration is not new and has been extensively used both in the boiling literature since the pioneering work of Nukiyama [9], and later in the stability limit context initiated by Skripov [10] and followed by numerous work [11–14]. In particular, Glod et al. [15] have successfully investigated the onset of boiling in water in this simple configuration. They were able to capture frames synchronized with the onset of boiling assuming a reproducible event of nucleation for multiple runs. In most of these works however, the heating rate is very large (about 10^7 K/s) so that only the immediate vicinity of the wire is

* Corresponding author. Tel.: +33 438 78 28 72.
E-mail addresses: Cedric.Poulain@cea.fr (C. Poulain), Jerome.Duplat@ujf-grenoble.fr (J. Duplat).

0017-9310/$ - see front matter © 2012 Published by Elsevier Ltd.
http://dx.doi.org/10.1016/j.ijheatmasstransfer.2012.06.095

overheated. For these reasons, a quantitative analysis of the acquired images remains quite difficult.

In this paper, high speed imaging as well as acoustics are employed to render the instantaneous vapour volume and to track the bubble dynamics at the nucleation instant on a single run in liquid ethanol. The heating rates used are relatively slow (about 10^4 K/s) so that most part of the energy is stored in the liquid, making the track of the nucleation process easier. This highly reproducible nucleation event will be examined as well as the following dynamic when the bubble gives birth to two vapour sheaths propagating towards overheated regions aside the bubble. As we will show, those sheaths propagate by vaporization of the overheated (metastable) liquid region surrounding the wire.

The paper is organized in the following way: The experimental setup as well as the technical acoustics and imaging means implemented to track the bubble dynamics are presented in the first section. This section also describes the technical procedure employed to analyze the data and get, for instance, the bubble volume or pressure. Section 3 is devoted to the comparison between the experimental temperature evolution measured before the onset of nucleation and the theoretical predictions obtained via a simple model. Boundary layer thickness as well as the associated energy storage are also discussed in this section. Section 4 details the vapour dynamics (after onset) analysed by video imaging. Mechanisms at play in this dynamics are emphasized and some predictions upon the pattern geometry are outlined. The main results are discussed in the last section.

2. Experimental procedure

2.1. Experimental Setup

The experimental setup (see Fig. 1) consists in a thin platinum wire immersed in liquid ethanol. A current I flows across the wire, leading to heat production by Joule effect and consequently to the surrounding liquid heating.

Before a set of experiments, the bulk of ethanol (96% purity) is boiled for several minutes, following the classical procedure for boiling experiments presumably to remove condensed gases. Experiments were carried out for several bulk temperature varying from 0 to 55 degrees below saturation temperature. For experiments run above room temperature, the bulk temperature is regulated by means of a dedicated electrical resistance, which is turned off just before the experimental run. One set of experiments was performed at temperature below the room temperature. In this case cold ethanol was prepared in a refrigerator, and was used without any other precautions (no regulation). The large dimensions of the ethanol vessel ($280 \times 200 \times 150$ mm), allow a satisfactory thermal stability (±1 K) during the experimental run set. The results presented in this paper are highly reproducible, which supports the choice of ethanol as well as this above described preparation procedure. Physical properties are given in Table 1.

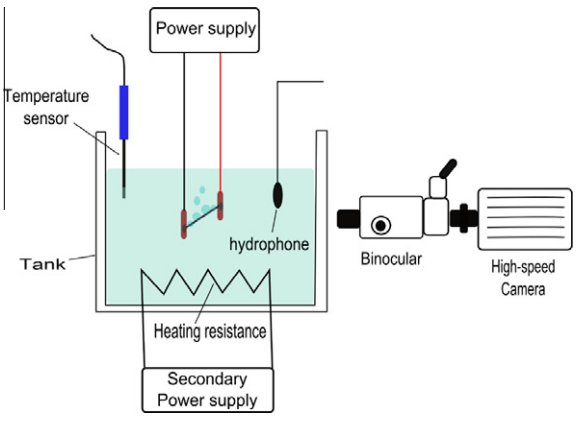

Fig. 1. Experimental setup.

Platinum wires (Goodfellow, 99.9% purity) of diameter 10 μm or 25 μm and lengths ranging from 4.5 to 32 mm were used as heating elements. Both ends of the wire were tin-welded to much larger section copper wires (2.5 mm^2). This electric cell is connected via a 4-wire wiring to a potentiostat-galvanostat (Biologic SP300, 48 V, 1.2 A max.). This system allows for fast and accurate regulation (up to 3 ms) as well as measurement (up to 5 kHz) of both the potential drop and the current in the platinum wire. Actually, the potensiostat probes the overall potential drop at both ends of the electric cell (Pt wire, Tin soldering and Copper wires) but the total voltage does not differ more than 0.1% from that of the platinum wire only.

In the present work, we use the potentiostat in a power controlled manner so that the power $\mathscr{P} = \mathscr{U}I$ imposed to the heating wire is constant whatever the voltage or current (or resistance) of the cell. The linear power density $P_\ell = P/\ell$ (with ℓ the wire length) is varied from 35 W/m to 75 W/m and from 85 W/m to 150 W/m for 10 μm and 25 μm wire respectively. This corresponds to surface power density up to 2.4 MW/m^2. The current I and voltage V are sampled at a rate of 5 kHz.

The nucleation process is visualised by means of a fast camera (Photron, FASTCAM SA1.1) mounted on a binocular (Olympus, SZX16). Fields of view are typically of 4×1 mm^2 were obtained with resolution 384×96 pixels, and recorded at frame rate as large as 120,000 frames per second (fps). The whole scene is backlighted with a 240 W cold light (Dedocool). A calibrated hydrophone (Bruel & Kjaer Type 8103), located in the vessel 4 cm away from the wire enables acoustic measurements during the nucleation process. The hydrophone is linked to a charge amplifier (Bruel & Kjaer, Nexus), whose voltage is proportionnal to the acoustic pressure P (typically 10 mV/Pa) within the frequency range 0–100 kHz. The output signal is recorded at a rate of 5 MHz with an oscilloscope (Tektronix, DPO 4032).

Finally, it is noteworthy that all those apparatus (potentiostat, camera and hydrophone) are synchronised thanks to the potentiostat trigger output.

2.2. Typical scenario

Initially, the liquid ethanol is at rest and at homogeneous temperature T_{bulk}. At time $t = 0$, a constant power is injected through the wire, heating the wire by Joule effect. Subsequently the ethanol in the vicinity of the wire is also heated.

Provided that the temperature is high enough, a vapour nucleus may appear at time t^* (or the order of 10 to 100 ms) which first grows spherically with a much faster dynamic (of the order of 10 μs). It is useful to introduce a new time origin, and we define $\delta t = t - t^*$ (see Eq. 14). Further on, lateral sheaths appear after a few microseconds and develop along the platinum wire. The whole gas bubble ultimately collapses and disappears. At this stage, nucleate or film boiling is responsible for the heat exchange between wire and liquid bulk, depending on the heat flux intensity. Screenshots of the typical phases of this process are shown on Fig. 2.

2.3. Data processing

2.3.1. Wire temperature determination

The instantaneous measurement of voltage U and current I allows to determine the wire resistance $\mathscr{R}_w = U/I$ which is a function of the mean wire temperature. By comparison with the resistance

Table 1
Properties of ethanol at atmospheric pressure (from [25,17]).

	k[W/m K]	ρ[kg/m^3]	C_p[kJ/(kg K)]	L_v[kJ/kg]	μ[Pa s]	ρ_v[kg/m^3]	β[K^{-1}]
$T_{sat} - 55\ K$	0.167	789	2.44	–	–	–	–
T_{sat}	0.153	757	3	963	428.7×10^{-6}	1.435	1.8×10^{-3}

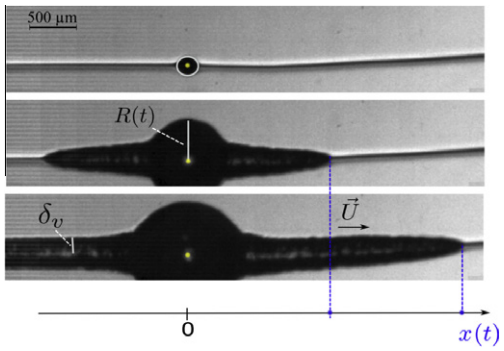

Fig. 2. Definition of the geometric properties of the central bubble and sheath for time $\delta t = 9, 72, 154$ µs after the onset at $T_{bulk} = T_{sat}$ on a 10 µm platinum wire ($\mathscr{P}_\ell = 58$ W/m).

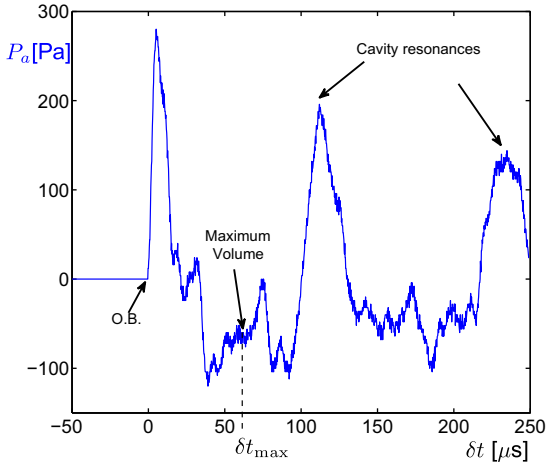

Fig. 3. Typical acoustic pressure signal recorded during the initial boiling event on a 10 µm Pt wire heated by Joule effect with a constant linear power of 67 W/m in liquid ethanol at $T_{bulk} = T_{sat} - 55$ K.

at room temperature, the wire average temperature can be deduced. Namely, it is known that Platinum resistivity and temperature are linearly related [15]:

$$T = 2.72 \times 10^9 \rho_e - 2, \quad \rho_e = \frac{\mathscr{R}_w S_e}{\ell}, \tag{1}$$

where temperature T is expressed in $[K]$ electrical resistivity ρ_e in $[\Omega\ \mathrm{m}]$ and wire cross section S_e in $[\mathrm{m}^2]$. However the platinum wire ends being welded to the thermalized copper wire, the measured temperature slightly underestimates the local temperature where nucleation occurs. We estimate the error is less than 2% of the wire overheating.

2.3.2. Image processing

For a given set of images in the nucleation regime, a simple threshold algorithm is applied to get the bubble's dimensions. In the initial stage (see Fig. 2, , top image), a spherical bubble is observed. The bubble's center and instantaneous radius $R(\delta t)$ are determined by matching a circle on the bubble contour. Subsequently, lateral sheaths appear and the same procedure can no longer be applied. In this case it is assumed that the bubble's center does not move. The radius of the main bubble is now defined as the transverse thickness of the central bubble (orthogonal to the wire axis). The lateral extension of the vapour sheath is easily obtained by intersecting the bubble contour with the wire (see Fig. 2, , bottom image).

2.3.3. Acoustic analysis

As mentioned earlier, the sound is also recorded during the onset. Indeed, just after the nucleation, i.e. the initial time at which some interface is created and gives rise to a rapidly expanding bubble, an acoustic wave is generated in the surrounding medium, which produces an audible sound. For a hydrophone located at a distance r away from the source, the acoustic signal is composed of the superposition of the waves generated by the bubble (acoustic source) and by its echoes at the tank wall (Fig. 3). For that reason, the acoustic analysis is restricted to the first instants (typically $\delta t \leqslant 100\ \mu s$) before any echo occurs. The distance $r = 4$ cm is chosen as a trade-off to have no echoes during the bubble's growth and to be compatible with the camera field of view.

For a arbitrary shaped body of variable volume $V(\delta t)$, it has been shown by Landau [16] that the far-field acoustic pressure $P_a(r, \delta t)$ at a distance r from the body is proportional to the volume second time derivative according to:

$$P_a(r, \delta t) = P(r, \delta t) - P_{bulk} = \frac{\rho}{4\pi r} \ddot{V}\left(\delta t - \frac{r}{c_s}\right), \tag{2}$$

where $c_s = 1200$ m/s is the speed of sound in ethanol [17], so that the bubble's volume can be readily obtained by a double integration of the acoustic signal. A comparison of this method with the direct optical one (video imaging) at the inital times of the nucleation process is illustrated on Fig. 4. The time origin $\delta t = 0$ of the event has been chosen at first non-zero acoustic signal. The advantage of this acoustic technique is two-fold: first the acquisition frequency is higher, second it provides a direct estimation of $\ddot{V}$, a quantity useful for determining the bubble inner pressure (see Eq. 3), which could hardly be obtained by a double derivation of $V(\delta t)$.

2.3.4. Rayleigh–Plesset

Just after the first nucleus has appeared (typ. $\delta t \leqslant 20$ µs), the vapour bubble rapidly grows with a shape remaining spherical. During this phase, the bubble expands with a radial outward flow in the surrounding liquid. While the flow is purely radial, the pressure $P_i(\delta t)$ at the vapour interface is governed by the Rayleigh–Plesset equation [18,19]. In the (V, P) frame, it can be written as:

$$P_i(t) = P_{bulk} + \rho\left(\frac{\ddot{V}}{4\pi R} - \frac{1}{2(4\pi)^2}\frac{\dot{V}^2}{R^4}\right), \tag{3}$$

The advantage of this frame is the explicit $\ddot{V}$ term that we get by acoustics. We thus obtain a measurement of the pressure at the bubble interface, which differs from the bubble inner pressure by two negligible terms. Indeed both the Laplace pressure drop $\Delta P = 2\sigma/R$ and the recoil pressure $P_r = (1/\rho_v - 1/\rho)(\dot{m}/A)^2 \approx \rho_v \dot{R}^2$ are small compared with the typical overpressure at the interface ($\rho \dot{R}^2$). Viscous effects have also been neglected (typical Reynols

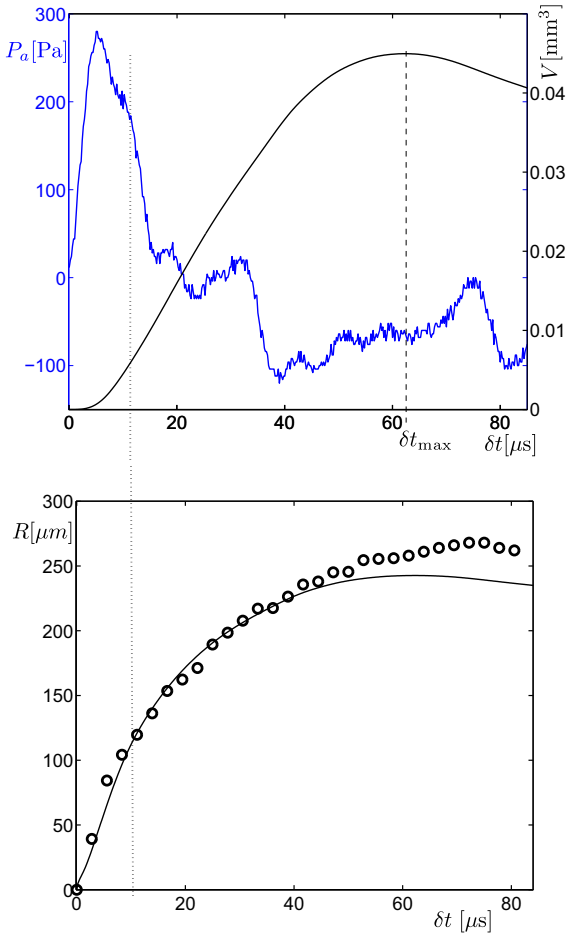

Fig. 4. Top: Acoustic pressure and corresponding nucleus volume obtained by Eq. (2) for $\mathscr{P}_\ell = 67$ W/m (Pt, 10 μm). Bottom: Corresponding radius estimated from whether acoustics (continuous line) or image processing (black circles). The black vertical dotted-line indicates the birth of sheaths.

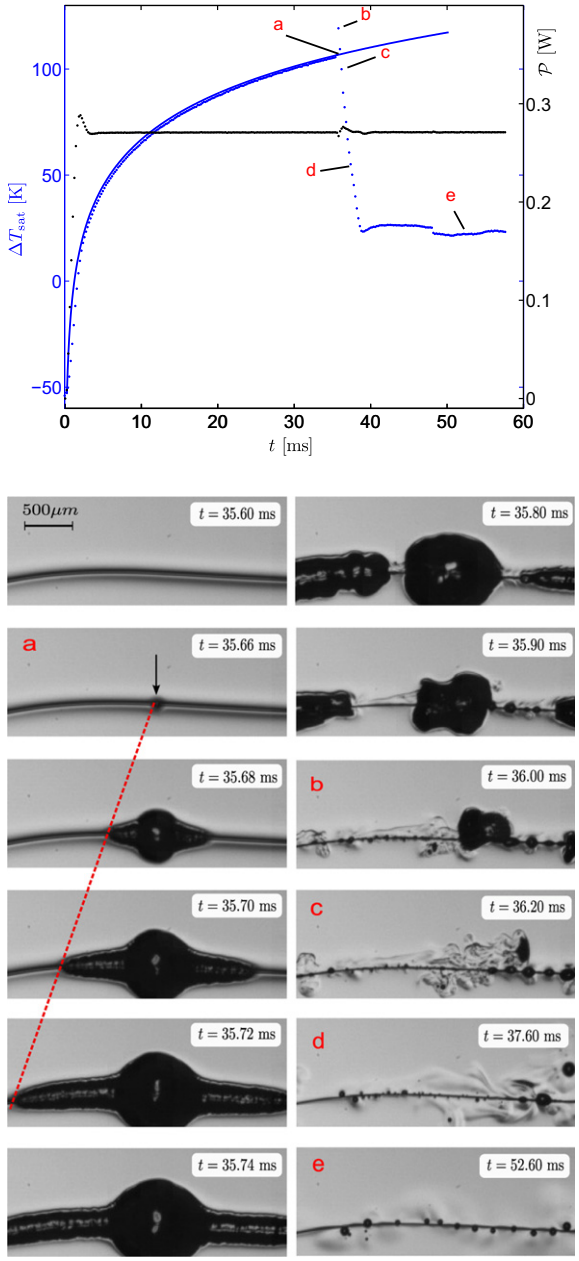

Fig. 5. Top: Temporal temperature evolution at the onset for a 10 μm Pt wire under a linear density power of 59 W/m ($1.88\,MW/m^2$) in ethyl alcohol at $T_{bulk} = T_{sat} - 55$ K. The continuous line corresponds to the prediction of Eq. (10). Bottom: corresponding sequence of the nucleation process.

number being of order 1000). The temperature can be deduced by assuming the gas is at saturation temperature.

To sum up, this procedure enables us to get an estimation of all the major thermodynamic quantities at play during the bubble growth. Namely, the instantaneous bubble volume $V(t)$ (as well as its time derivatives) are obtained thanks to acoustic measurements Eq. (2). Then, those quantities are injected in the Rayleigh–Plesset Eq. (3) to get the pressure inside the bubble.

3. Temperature field

3.1. Typical temperature evolution

For every experimental run, the wire and bulk temperature are initially homogeneous ($T_{bulk} = T_w$). The typical wire temperature evolution after heat is supplied ($t = 0$), together with the corresponding snapshots is shown on Fig. 5.

First, in the liquid-only phase regime (before the nucleation onset), the temperature rapidly increases with a decreasing slope in time. Then, the temperature evolution becomes more complicated once the nucleation process has started: just after nucleation, the temperature rapidly increases, over a period coinciding with the development of the central bubble and the vapour sheath. After they have collapsed, the temperature reaches a plateau. The final temperature depends on experimental conditions. In this phase, two boiling processes might be observed depending on those conditions: either nucleate boiling (NB) or film boiling (FB) take place leading respectively to a plateau temperature of a few degrees over T_{sat} or more than 300 K. The prediction of the final overtemperature is given by one or another branch of the Nukiyama curve but is beyond the scope of this paper mainly focusing on the nucleation process and we will discuss only the temperature evolution until the vapour nucleus appear.

3.2. Nucleation temperature

Typical temperature evolution for several linear power are shown on Fig. 6. The magnitude of temperature elevation is proportional to the input power, and is faster for small wire diameters. Fig. 6 shows that all experiments have an universal behavior when

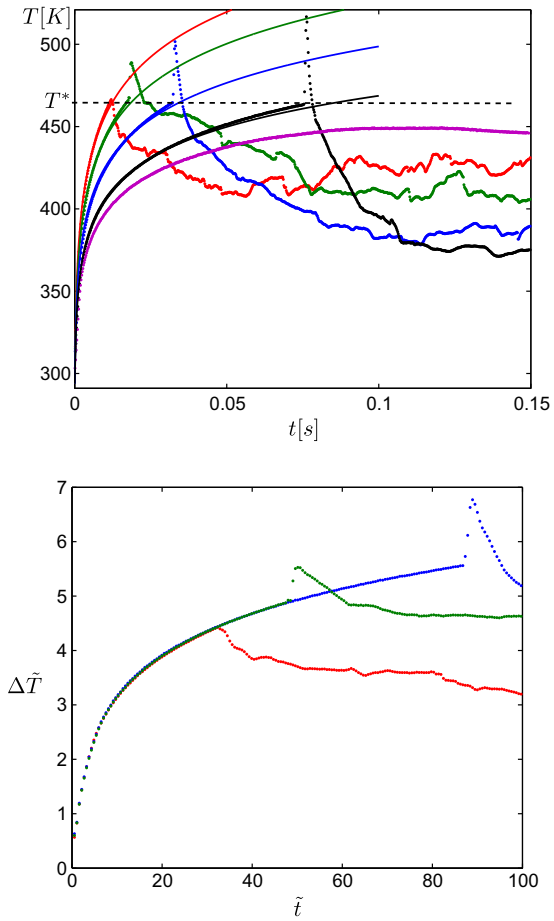

Fig. 6. Top: temperature evolution of a 10 μm Pt wire in ethanol ($T_{bulk} = 298$ K) for decreasing power input ($\mathscr{P}_\ell = 75$(red), 68(green), 59(blue), 52(black) and 50(purple) W/m). For the weaker input power, the wire temperature is eventually cooled by the onset of natural convection and therefore no nucleation is observed. Continuous lines correspond to Eq. (10). Bottom: Non dimensional representation of the former plot.

temperature and time are made non dimensional according to the scaling:

$$\tilde{T} = \frac{4\pi k}{\mathscr{P}_\ell}(T - T_{bulk}), \quad \tilde{t} = t\frac{4\alpha}{d^2}. \tag{4}$$

As can be seen on Fig. 6, this temperature elevation stops as soon as one or the other of these events happens:

- For low power input, the temperature reaches a maximum followed by a decrease owing the onset of natural convection [20]. In this case, no boiling is ever observed even for wire temperature far above saturation temperature. This case will no longer be mentioned in this paper, as we focus on the phase change process.
- For larger power input the temperature increases until a vapour germ appears at incipience time t^*.

It is noteworthy that, whatever the conditions (power, wire diameter and length, bulk temperature...), this nucleation process occurs when the wire temperature reaches

$$T^* = 465 \pm 2 \text{ K}, \tag{5}$$

114 K above saturation temperature.

3.3. Model for the temperature before incipience of boiling

Initially, the wire and the surrounding liquid are at equilibrium so that their temperature is homogeneous at T_{bulk}. Afterwards, heat is dissipated within the wire and diffuses through the liquid. Let us first assume that the wire is infinitely long and that no natural convection is triggered. The spatio-temporal field of temperature is thus an axisymmetric purely diffusive problem obeying:

$$\begin{cases} \frac{\partial T}{\partial t} + \alpha_w \frac{\partial}{r\partial r} r \frac{\partial T}{\partial r} = \frac{4\mathscr{P}_\ell}{\pi d^2 \rho_w C_{P,w}} & r < d/2, \\ \frac{\partial T}{\partial t} + \alpha \frac{\partial}{r\partial r} r \frac{\partial T}{\partial r} = 0 & r > d/2, \\ k_w \frac{\partial T}{\partial r}\big|_{r=(d/2)^-} = k \frac{\partial T}{\partial r}\big|_{r=(d/2)^+}, \\ T(r,0) = T_{bulk}. \end{cases} \tag{6}$$

This complete set of equation does not exhibit any trivial analytical solution, and can only be solved numerically. However, one may consider the two following simplifications:

Firstly, let us assume that the heat source (the wire) is infinitely thin (no radial extension) located at $r = 0$. Hence, heat is exchanged with the surrounding liquid via a boundary layer that grows diffusively with time: $\delta_T \approx 2\sqrt{\alpha t}$. Let us define a transient heat exchange coefficient h as: $h = k/\delta_T$ so that the Biot number associated with the wire writes:

$$Bi = \frac{hd}{2k_w} = \frac{k}{k_w}\frac{d}{4\sqrt{\alpha t}}, \tag{7}$$

which turns out to be small as soon as $t > (k/k_w)^2 d^2/16/\alpha \approx 0.4$ ns for a 10 μm wire. Thus, the wire temperature can be considered as homogeneous after a very short time. Secondly, let us show that the specific energy stored into the wire is negligible in comparison with that stored in the liquid for the wires used in our experiments:

The heat capacity of the wire per unit length is: $C_w = \rho_w\ C_{Pw}\pi d^2/4$. At time t, the heat has spread in the liquid over a distance δ_T so that the heat capacity of the liquid is $C_\ell = \rho C_P \pi \delta_T^2$. The former is negligible for any time t such that:

$$t \gg \frac{\rho_w C_{P,w}}{\rho C_P}\frac{d^2}{4\alpha}. \tag{8}$$

which yields, $t = 0.5$ ms for a 10 μm wire and $t = 3$ ms for a 25 μm wire.

These times are short in comparison with the incipience time t^*, so that the specific contribution of the wire in the heat distribution is negligible, and that the complete problem may be approached by considering an homogeneous medium, heated on a line at $r = 0$. The solution of this simplified model matches with the complete one for all $r > d/2$, and the temperature of the wire is approached by the temperature of the interface ($T(d/2,t)$). For this simplified problem the solution is [21]:

$$T(r,t) - T_{bulk} = \frac{\mathscr{P}_\ell}{4\pi k}\int_{\frac{r^2}{4\alpha t}}^{\infty}\frac{e^{-u}}{u}du = \frac{\mathscr{P}_\ell}{4\pi k}E_1\left(\frac{r^2}{4\alpha t}\right), \tag{9}$$

where E_1 is the exponential integral function of order 1. For the particular case $r = d/2$ (wire skin), it gives :

$$T_w(t) = \frac{\mathscr{P}_\ell}{4\pi k}E_1\left(\frac{d^2}{16\alpha t}\right), \tag{10}$$

We have checked that the numerical solution of the complete set of Eqs. 6 matches the prediction of this simplified model with an agreement better than 1% and matches well the experimental results (Fig. 6 top). The purely diffusive heat transfer assumption in the liquid is valid provided nucleation occurs at a time t^* smaller than the time t_{cv} at which convection transfer becomes dominant. The instant t_{cv} can be estimated by [22]:

$$t > t_{cv} = 43\left(\frac{g\beta\sqrt{\alpha}\mathscr{P}_\ell}{k\nu}\right)^{-2/3} \tag{11}$$

decreases with the heat flux, so that for high enough input power, t_{cv} becomes larger than t^* and no convection develops. On the contrary, when the heat power is not high enough, convection starts and cools the wire so that no nucleation can be triggered, as can be seen on Fig. 6. Assuming the temperature field prediction (Eq. (10)), t^* can be written as:

$$t^* = \frac{d^2}{16\alpha}E_1^{-1}\left(\frac{4\pi k\Delta T^*}{\mathscr{P}_\ell}\right)$$

with $\Delta T^* = T^* - T_{\text{bulk}}$. The expression of t^* can be approximated by [21]:

$$t^* \approx \frac{d^2}{16\alpha}\exp\left(\frac{4\pi k\Delta T^*}{\mathscr{P}_\ell} + 0.57721\right), \tag{12}$$

in a good agreement with experimental data (Fig. 7).

3.4. Energy storage

At time t^* a vapour nucleus appears and expands in the overheated liquid whose temperature profile is determined by Eq. (9). Let us introduce $E_{s,}$ the amount of specific energy stored by the liquid per unit length, at a temperature above the saturation temperature:

$$E_{s,} = 2\pi C_p\rho\int_{\frac{d}{2}}^{\frac{d}{2}+\delta_{\text{sat}}} r(T(r,t^*) - T_{\text{sat}})dr, \tag{13}$$

where δ_{sat} is the thickness of the overheated region (i.e. where $T(r,t^*) > T_{\text{sat}}$, see Fig. 8).

The total energy stored $E_{s,}$ is an increasing function of the boundary layer thickness, and then of time t^*. Consequently, it is a decreasing function of the input power P_ℓ, which can seem contradictory at first sight.

Thanks to this modeling the system state is perfectly known at incipience instant t^*.

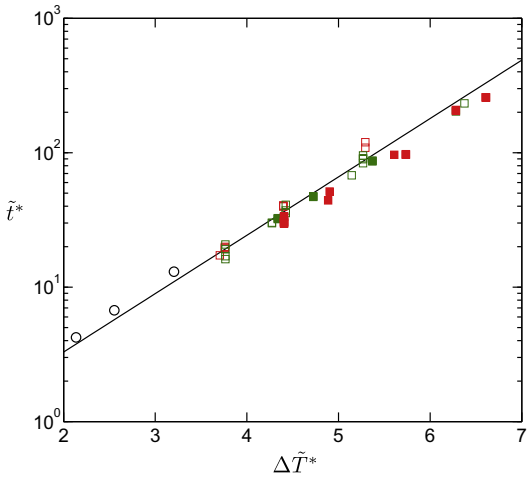

Fig. 7. Dimensionless nucleation time as a function of dimensionless nucleation temperature. Green squares represent a 10 μm Pt wire diameter and 18 mm length at $T_{\text{bulk}} = T_{\text{sat}} - 55$ K (full ones) and $T_{\text{bulk}} = T_{\text{sat}}$ (empty ones). Red squares represent a 10 μm Pt wire diameter and 6 mm length at $T_{\text{bulk}} = T_{\text{sat}} - 55$ K (full ones) and $T_{\text{bulk}} = T_{\text{sat}}$ (empty ones). Empty Circles represent a 25 μm Pt wire diameter and 9 mm length at $T_{\text{bulk}} = T_{\text{sat}} - 55$ K. The black line represents the exponential law $\tilde{t}^* = 0.25\exp\left(\Delta\tilde{T}^* + 0.57721\right)$.

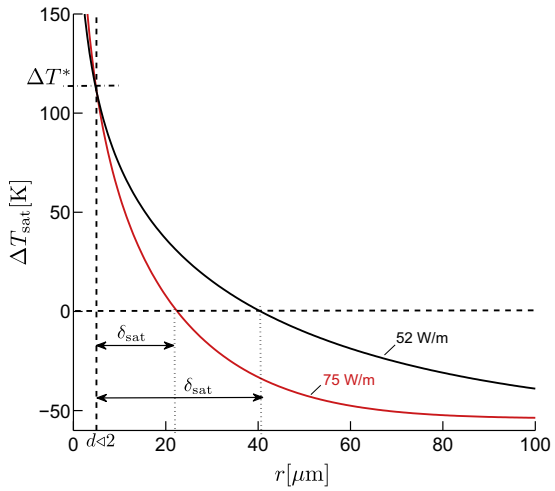

Fig. 8. Temperature profiles given by Eq. (9) at boiling incipience for $\mathscr{P}_\ell = 75$ W/m (red), $\mathscr{P}_\ell = 52$ W/m (black) at $T_{\text{bulk}} = T_{\text{sat}} - 55$ K.

4. Vapour dynamics

In this part, we will detail the mechanism of expansion of the first vapour bubble just *after* the phase transition has occurred. At the onset, a nucleus quickly grows over a time of typically 100 μs, a time much shorter than t^*. As described above (see Fig. 5) the development of this bubble proceeds in two stages: in the first instants, the bubble remains perfectly spherical. After a few microseconds, lateral sheaths grow in the wire direction, when the central part continue to grow. The maximum radius is reached at the instant when both sheaths detach from the central bubble. As said above, t^* will be taken as the new origin of time, and time will be denoted δt

$$\delta t = t - t^*. \tag{14}$$

4.1. Before shealths appear

The trajectory $R(\delta t)$ of the central bubble radius is measured both by optical and acoustical means. These independent measurements are in good agreement (Fig. 4), at least for the initial instants when the bubble keeps its spherical symmetry. Further on, the assumption $V = 4/3\pi R^3$ is no longer valid so that some discrepancies are observed.

The short-time dynamics (typically for $\delta t < 10$ μs) remains unchanged whatever the experimental conditions. Namely, the initial velocity value: $\dot{R}_0 \approx 10$ m/s is independent on experimental conditions (linear power, bulk temperature, wire diameter). Accordingly the inner pressure evolution is also universal. A sharp pressure peak is observed at the bubble nucleation: the over pressure is 1.5 bar during 10 μs. After this initial nucleation process, the central bubble continues to grow at ambient pressure (see 4.4)

4.2. Lateral sheath propagation

At the end of the initial nucleation process, two outgrowths of vapour are visible at the side of the bubble (along the wire) and break the spherical symmetry. These outgrowths propagate along the heating wire, so that a sheath of vapour surrounds the wire. The propagation velocity is constant within a single run but typically varies from 15 to 19 m/s from an experiment to another although measured with a very high confidence ($\sim 1\%$). Geometrically, the sheath can be described as a cylindrical part connected to a conical tip. The sheath tip shape is also universal and has a curvature radius $a \approx 40$ μm (see Fig. 2).

The mean radius δ_v of the cylindrical part of the sheath can be clearly identified and is measured directly on the recorded images. It ranges from 60 to 300 microns. δ_v is smaller for increasing linear power $\mathscr{P}_\ell$ and larger for larger wire diameter. These trends can be summarized by noticing that δ_v is an increasing function of t^*.

More precisely, if we compare the specific energy per unit length stored in the liquid $E_{s,}$ (see 3.4), with the latent energy used to create the vapour sheath and given that $2\delta_v \gg d$, it follows that:

$$Q_\ell = \pi\delta_v^2\rho_v L, \tag{15}$$

which yields, for our experiments (see Fig. 9) to

$$Q_\ell \approx 0.25E_{s,} \tag{16}$$

indicating that the sheath expansion is fed by the sensitive energy stored in the liquid.

4.3. Sheath detachment

The sheaths propagate until they reach the wire ends. However they detach from the central bubble at time $\delta t_{\max}$. $\delta t_{\max}$ increases with δ_v. Fig. 10 shows that

$$\delta t_{\max} \approx 0.52\left(\frac{\rho\delta_v^3}{\sigma}\right)^{1/2} = 0.4\tau_c, \tag{17}$$

where σ stands for the ethanol surface tension, and τ_c is the time-scales of the Plateau instability [23].

Fig. 11 shows the pinch-off dynamics obtained by means of high speed imaging. The neck diameter δ_n vanishes singularly in a finite time: introducing the countdown time $\tau = \delta t_{\max} - \delta t$ before detachment, one gets:

$$\frac{\delta_n}{\delta_v} = p\left(\frac{\tau}{\delta t_{\max}}\right)^{1/2}, \text{ with } p = 1.0, \tag{18}$$

in good agreement with the pinch-off dynamics of gas tubes in liquids [24] for which $p = 0.88$. The sheath detachment is thus a capillary-driven process. Consequently, the time during which the sheath remains connected to the central bubble is governed by this capillary time τ_c.

4.4. Central bubble dynamics

As seen on Fig. 4, the bubble volume is quasi linear after the sheaths have appeared, and until the bubble begins to collapse.

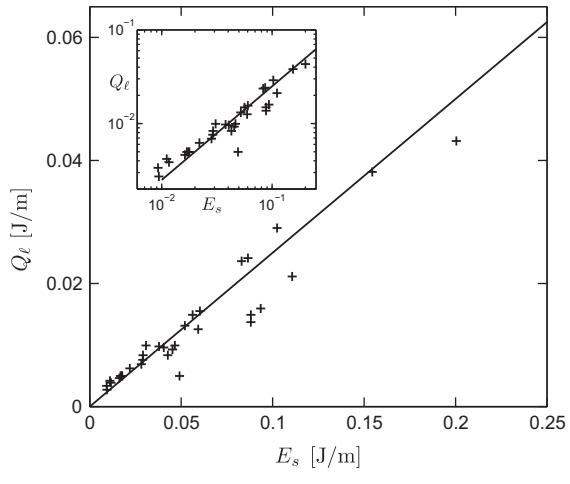

Fig. 9. Latent heat required for the sheath creation as a function of specific heat stored in the superheated region surrounding the wire. Insert: same graph in log-log coordinates. The black line is the graphic representation of $Q_\ell = 0.25E_{s,}$.

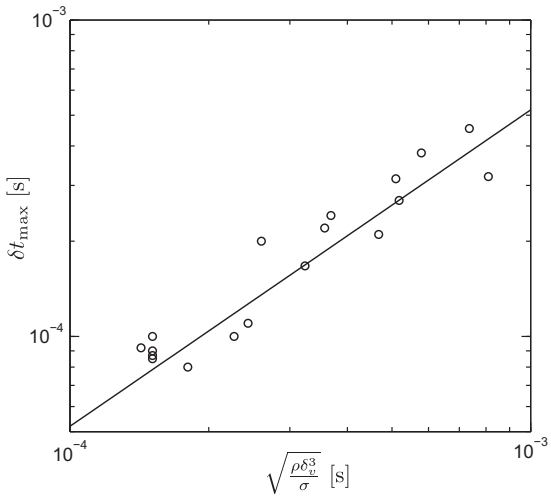

Fig. 10. Detachment time $\delta t_{\max}$ for several sheath thickness δ_v for a 10 μm Pt wire. The continuous line represents the Eq. (17).

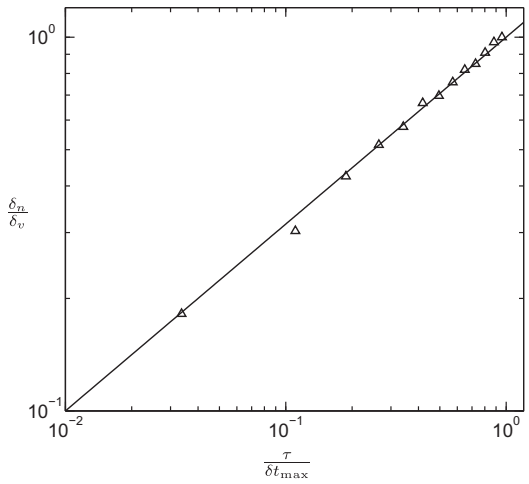

Fig. 11. Time evolution of the neck diameter during the pinch-off process in ethanol at $T_{\text{bulk}} = T_{\text{sat}}$ and $\mathscr{P}_\ell = 58$ W/m. The continuous line corresponds to Eq. (18).

Its maximum radius $R_{\max}$ is reached at time $\delta t_{\max}$ which coincides with the pinch-off instant. At this time the vapour can no longer flow from sheaths to the central bubble. (Fig. 12).

It is also noteworthy that, in this linear regime, the bubble expands with an inner pressure that hardly equals the ambient pressure. These remarks strongly suggest that the central bubble is fed by the propagating sheaths with a constant mass rate, before it collapses when they detach. Indeed, the radius $R_{\max}$ is much larger than the vapour sheath thickness δ_v, so that the latent energy

$$Q_{\max} = \frac{4\pi}{3}R_{\max}^3\rho_v L, \tag{19}$$

that is necessary to vaporize the central bubble is much larger than the specific heat that is locally available ($2R_{\max}E_{s,\ell}$). As can be seen on Fig. 13, $Q_{\max}$ is comparable with the energy $E_{\max}$ stored along the wire, on the length over which sheaths propagate before detachment:

$$E_{\max} = E_{s,\ell}2U\delta t_{\max}. \tag{20}$$

More precisely, we have observed that whatever the linear power or bulk temperature, we have

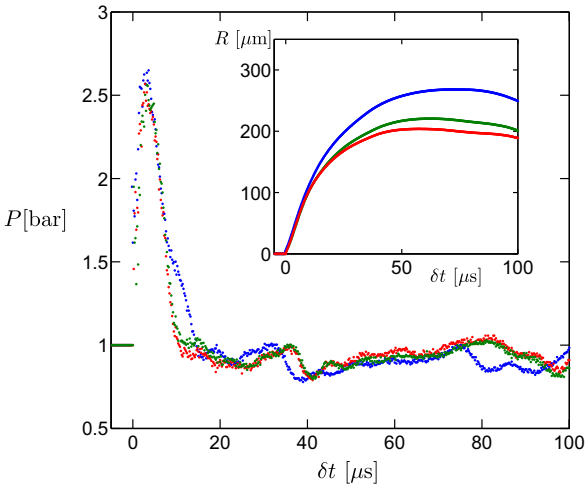

Fig. 12. Inner pressure evolution after the onset for three linear powers ($\mathscr{P}_\ell$ =75(red), 68(green), 60(blue) W/m) at $T_{bulk} = T_{sat} - 55$ K. Insert: corresponding central bubble radii (acoustic estimation).

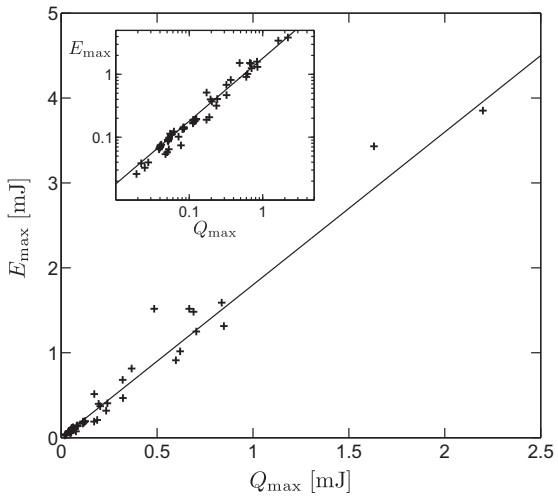

Fig. 13. Specific energy stored on the length encountered by the sheaths before detachment as a function of the latent heat required for bubble vaporisation. Insert: same graph in log-log coordinates. The continuous line corresponds to Eq. (21).

$$Q_{max} \approx 0.56 E_{max}. \quad (21)$$

In other words, the main bubble diameter would not be so large if it only used the specific energy locally available. While they keep connected to the main bubble, the sheaths act as vapor suppliers for it. The factor 0.56 probably underestimates the actual energy as the central bubble is slightly prolate at maximal expansion. On top of that, about a quarter of the specific energy is used for the sheath creation (see Eq. 16) so that overall, about 10% – 15% is missing. This supplementary energy is probably exchanged with the liquid bulk (thermal boundary layers are strongly deformed during the bubble expansion process, which is known to enhance conductive heat transfer) so that, after the onset of nucleation, the liquid surrounding the wire is cooled and reaches a stationary state with a temperature given by the Nukyama curve for the imposed heat flux.

5. Further remarks and conclusion

In this paper, we have reported experiments on rapid vaporization dynamics that occurs at the onset of nucleation when the first bubble appears in a liquid before boiling. In our experiments for which a thin wire is relatively slowly heated by Joule effect, nucleation occurs via a very reproducible process: a main bubble (which we call the central bubble) is created and rapidly grows. Lateral sheaths are created because of the heat stored in the liquid surrounding the wire. Given the relatively slow heating rate we used, a great part of the energy is stored in the liquid in metastable state. When the first nucleus appears and the central bubble grows, the overheated metastable liquid is in contact with a vapor interface. The (meta)stability is broken and liquid vaporizes. The interface propagates from the central bubble towards the overheated region along the wire.

We have observed that whatever the bulk temperature and the temperature rise rate tested, nucleation starts at a constant temperature of about 465 K in liquid ethanol, very close to the spinodal one (T=470 K). The initial overpressure within the bubble measured by acoustics is also constant and (about 1.6 bar), whatever the maximum bubble size reached (R_{max}). Thanks to a simple model for predicting the instantaneous temperature profile around the heating wire, we have shown that the bubble maximum size is a function of the amount of specific energy stored in the liquid (above saturation). The bubble maximum size is namely larger for smaller heat fluxes since the boundary layer gets thicker for slower temperature rise rate. More precisely, after its creation the bubble is fed at a constant mass rate by the sheath propagating at constant velocity. The bubble size is thus determined by the sheath extension at the time when they detach from the central bubble. As we have shown, the breakup time is determined by a Plateau-type instability which also drives the pinch-off dynamics. Our model is thus predictive on the time t^* at which onset is likely to happen, on the maximum bubble size R_{max}, as well as on the collapsing time δt_{max} when sheaths detach from the bubble).

However, the sheaths velocity as well as the bubble dynamics and overpressure at short time (≈ 20 μs) do not seem to depend strongly on experimental conditions tested. Overall, our conclusions on the bubble geometry as well as on the final pattern emphasize the importance of the temperature field, namely its non-homogeneity, in the large scale and long time nucleation process. More precisely, the knowledge of the temperature field (in space and time) is necessary to predict the final large scale pattern, although the nucleation conditions (temperature, bubble inner pressure, sheaths velocity) remain the same for our range of experiments. Further investigations will be necessary to understand and model the sheath propagation as well as this possibly universal very-short time bubble dynamics.

It is also noteworthy that the heating rate employed in this paper are about 1000 times smaller than those commonly used by other groups [15]. This much higher heating rate must account for the apparently different nucleation behavior. First, In Glod [15] experiments the temperature rise is so fast that the amount of energy stored in the liquid is negligible in comparison with the one stored in the wire and is thus independent on this rate. Consequently the amplitude of bubble maximal mechanical power is also found to be roughly independent on the temperature rise rate. Second, for slow heating rates, once a nucleus starts to develop, the temperature rise is slow enough and the sheath propagation so fast that no other bubble has time to develop. In other words, the first nucleus (so called central bubble) gives birth to two propagating vapor sheaths that recover the wire and also cool the wire. Thus, their development hinders any other nucleus to appear. Actually, for long enough wires, another 'central' bubble is likely to appear quasi simultaneously away from the first central bubble. Indeed the sheath propagation time is so large that the nucleation conditions might be reached at another location on the wire. Sheaths growing from each bubble are then likely to merge. With that scenario, the classical picture of quasi-simulta-

neously nucleating bubbles might be recovered for high enough heating rates.

Acknowledgements

We wish to thank C. Kevorkian for his precious technical help, as well as E. Hervieu for his scientific support.

Appendix A. Supplementary material

Supplementary data associated with this article can be found, in the online version, at http://dx.doi.org/10.1016/j.ijheatmasstransfer.2012.06.095.

References

[1] Pablo G. Debenedetti, Metastable Liquids, Concepts and Principles, Princeton University Press, 1996.
[2] T.D. Wheeler, A.D. Stroock, The transpiration of water at negative pressures in a synthetic tree, Int. J. Heat Mass Transfer 455 (2008) 208–212.
[3] J.C. Fisher, The fracture of liquids, J. Appl. Phys. 19 (1948) 1062–1067.
[4] E. Herbert, S. Balibar, F. Caupin, Cavitation pressure in water, Phys. Rev. E 74 (4) (2006) 041603.
[5] C.A. Ward, A. Balakrishnan, F.C. Hooper, On the thermodynamics of nucleation in weak gas–liquid solution, J. Basic Eng. 92 (4) (1970) 695–704.
[6] S.D. Lubetkin, Why is it much easier to nucleate gas bubbles than theory predicts?, Langmuir 19 (2003) 2575–2587
[7] V.G. Baidakov S.G. Protsenko, S.G. Protsenko, Metastable states in liquid–gas phase transition. Simulation by the method of molecular dynamics, High Temp. 41 (2) (2003) 195–200.
[8] C. Unal, V. Daw, R. Nelson, Unifying the controlling mechanisms for the critical heat flux and quenching: the ability of liquid to contact the hot surface, ASME J. Heat Transfer 114 (1992) 972–982.
[9] S. Nukiyama, The maximum and minimum values of the heat q transmitted from metal to boiling water under atmospheric pressure, Int. J. Heat Mass Transfer 9 (1934) 1419–1433. translated in 1966.
[10] V.P. Skripov, P.A. Pavlov, Explosive boiling of liquids and fluctuation nucleus of formation, High Temp. 8 (1970) 782.
[11] M-C Duluc, B. Stutz, M. Lallemand, Boiling incipience in liquid nitrogen induced by a step change in heat flux, Int. J. Heat Mass Transfer 51 (2008) 1738–1750.
[12] N. Bakhru, J.H. Lienhard, Boiling from small cylinders, Int. J. Heat Mass Transfer 15 (1972) 2011–2025.
[13] S.M. You, Y.S. Hong, J.P. O'Connor, The onset of film boiling on small cylinders: local dryout and hydrodynamic critical heat flux mechanisms, Int. J. Heat Mass Transfer 37 (1994) 2561–2569.
[14] K.P. Derewnicki, Experimental studies of heat transfer and vapour formation in fast transient boiling, Int. J. Heat Mass Transfer 28 (1985) 2085–2092.
[15] S. Glod, D. Poulikakos, Z. Zhao, G. Yadigaroglu, An investigation of microscale explosive vaporisation of water on an ultrathin pt wire, Int. J. Heat Mass Transfer 45 (2002) 367–379.
[16] L.D. Landau, E.M. Lifchitz, Physique Théorique, Mécanique des fluides, third ed., Ellipses, 1994.
[17] W.M. Mickey Haynes (Ed.), CRC Handbook of Chemistry and Physics, Internet Version, 91st ed., 2011.
[18] L. Rayleigh, On the pressure developed in a liquid during the collapse of a spherical cavity, Phil. Mag. 34 (200) (1917) 94–98.
[19] M.S. Plesset, A. Prosperetti, Bubble dynamics and cavitation, Ann. Rev. Fluid Mech. 9 (1) (1977) 145–185.
[20] M-C Duluc, S. Xin, P. Le Quéré, Transient natural convection and conjugate transients around a line heat source, Int. J. Heat Mass Transfer 46 (2003) 41–354.
[21] H.S. Carslaw, J.C. Jaeger, Conduction of Heat in Solids, second ed., Oxford University Press, 1959.
[22] C.M. Vest, M.L. Lawson, Onset of convection near a suddenly heated horizontal wire, Int. J. Heat Mass Transfer 15 (1972) 1281–1283.
[23] S. Chandrasekhar, Hydrodynamic and Hydromagnetic Stability, Oxford University Press, 1961.
[24] J.C. Burton, R. Waldrep, P. Taborek, Scaling and instabilities in bubble pinch-off, Phys. Rev. Lett. 94 (2005) 184502.
[25] Van P. Carey, Liquid–Vapor Phase-Change Phenomena, second ed., Taylor & Francis, 2008.